ADVANCED FUNCTIONAL MATERIALS
www.afm-journal.de

2D Ruddlesden-Popper versus 2D Dion-Jacobson Perovskites: Of the Importance of Determining the "True" Average *n*-Value of Annealed Layers

*Marie Cresp, Min Liu, Marie-Noelle Rager, Daming Zheng, and Thierry Pauporté**

2D Ruddlesden-Popper (RP) and Dion-Jacobson (DJ) halide perovskite structures are characterized by the *n* parameter that represents the number of PbI_6 layers in the spacer-separated perovskite slabs. In most of the literature, *n* is referred to the initial composition of the precursor solution and, then, to the initial spacer content. In this approach, the fact that the spacer can be partially lost upon annealing is not considered. Here, the chemical processes occurring upon the preparation of reduced-dimensional halide perovskite thin films of both families are investigated with a special focus on the organic cations composition and, especially, the evolution of *n* values. For each family, several spacers are investigated. It is shown that a large amount of monoammonium spacer cations is progressively eliminated upon annealing for the 2D-RP perovskites, while, on the contrary, the final composition is close to the initial one in the case of the diammonium spacer cations of the 2D-DJ perovskites. The elimination is related to the volatilization of the species after their deprotonation and the phenomenon can be regulated by halide additives. This work provides an important insight into the chemistry of the 2D perovskite layers and shows the importance of determining their "true" *n* value.

1. Introduction

2D halide perovskites (HPs) are focusing increasing attention in the research field of photovoltaic technologies.[1,2] Compared to their 3D counterparts, 2D perovskites have the advantage of being more stable against external stressors such as moisture, illumination, and heat due to the introduction of large organic spacer cations between the planes of inorganic slabs.[3,4] 3D perovskites can be described with the formula ABX_3, where A is an organic cation such as methylammonium (MA^+) or formamidinium (FA^+) or an inorganic cation such as cesium (Cs^+) or rubidium (Rb^+), B corresponds to a bivalent metal cation, usually Pb^{2+}, and X represents a halide anion, typically iodide (I^-), chloride (Cl^-), bromide (Br^-) and their mixtures.[5] 3D perovskites have a cubic symmetry where $[BX_6]^{4-}$ octahedral units are shared by their corners. However, a deviation from cubic symmetry is often encountered and can be attributed to several factors including the atomic sizes of the constituents. The FA-based photoactive α-$FAPbI_3$ phase can convert spontaneously into non-photoactive δ-$FAPbI_3$ phase in ambient conditions due to the large size of formamidinium cations.[6,7] One strategy to improve the stability of the α-$FAPbI_3$ phase is to use large cations in a small amount acting as additive[8–10] or in a larger amount creating layers of 2D perovskite.[11–14] 2D perovskites consist of alternating layers of organic cations and inorganic anionic frameworks forming a 2D lattice structure. The inorganic layers typically comprise metal halide octadedra $[BX_6]^{4-}$ interconnected by corner-sharing halide ions, while the organic cations are in between these inorganic layers.[15,16] The 2D Ruddlesden-Popper (RP) perovskites formula is $A'_2A_{n-1}B_nX_{3n+1}$ where A′ is a large monoammonium. RP perovskites use two monoammoniums bonded by van der Waals interactions to separate the inorganic frameworks. It leads to a half-octahedra displacement between the two inorganic layers due to steric hindrance and a large interlayer distance. On the contrary, the 2D Dion-Jacobson (DJ) perovskites formula is $A''A_{n-1}B_nX_{3n+1}$, where A″ is a large diammonium. DJ perovskites feature a continuous network of corner-sharing metal halide octahedra because divalent spacer cations are vertically bonded with adjacent slabs, resulting in well-aligned layered structures with an interlayer distance shorter than in their RP counterparts.[17] Therefore, the DJ halide perovskites present multiple significant advantages in terms of structural stability and carrier transport compared to the RP HP ones.

M. Cresp, M. Liu, D. Zheng, T. Pauporté
Institut de Recherche de Chimie Paris (IRCP)
Chimie ParisTech
PSL University
CNRS
UMR8247, 11 rue P. et M. Curie, Paris F-75005, France
E-mail: thierry.pauporte@chimieparistech.psl.eu
M.-N. Rager
Chimie ParisTech
PSL University
NMR Facility
11 rue P. et M. Curie, Paris F-75005, France

The ORCID identification number(s) for the author(s) of this article can be found under https://doi.org/10.1002/adfm.202413671

DOI: 10.1002/adfm.202413671

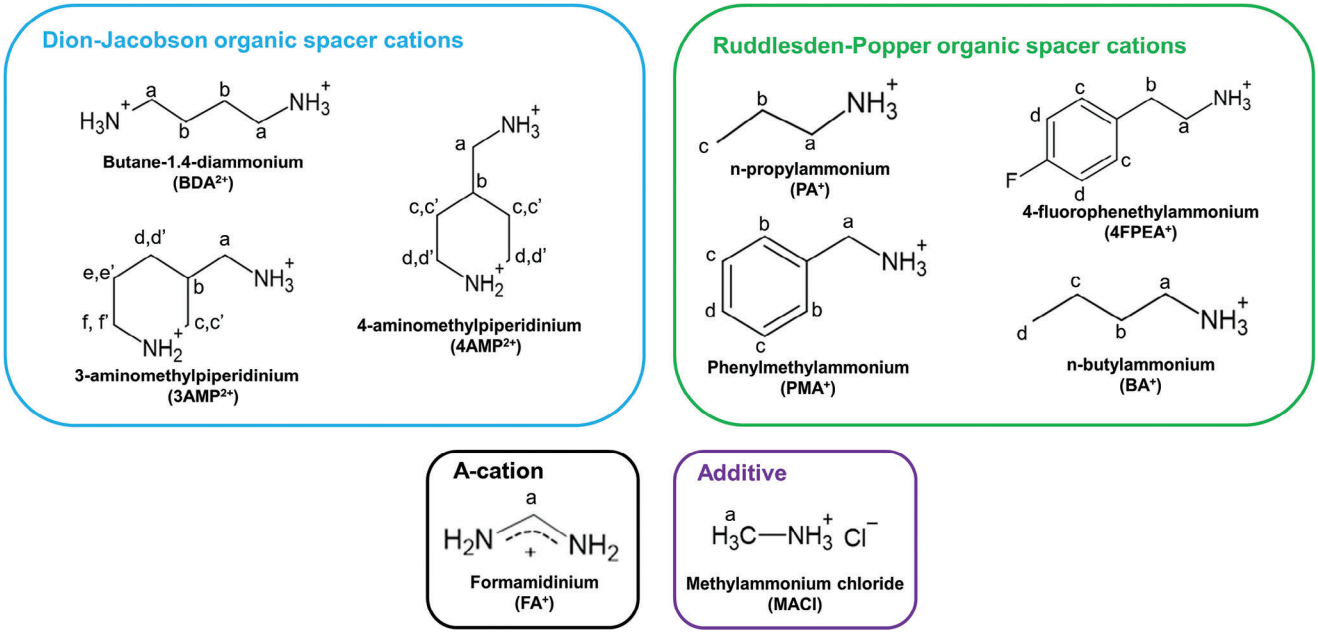

Figure 1. Chemical structures and proton indexation of organic cations used in 2D Dion-Jacobson and 2D Ruddlesden-Popper halide perovskites.

The number of structural inorganic layers in a slab is defined by the *n* parameter. This parameter plays a pivotal role in dictating the optoelectronic properties of the overall material. The manipulation of *n* enables the fine-tuning of key properties such as the exciton binding energy, the charge carrier mobility, and the optical absorption spectra.[18] However, this parameter remains ambiguous because of its multifaceted nature. First, it has been shown that for n higher than 1, the 2D perovskite films are usually composed of multiple perovskite phases of various *n* values. When one speaks about a 2D halide perovskite film composition it refers to the average of these *n* values. Second, in recent research articles, stoichiometric quantities of cations introduced into the perovskite precursor solution (PPS) are usually used to define the average *n* in the final layer of 2D PSCs.[19–27] It implies that the amount of cations introduced in the PPS is similar to the amount of cations in the final annealed film. However, it is well-known that some cations, initially introduced in the PPS as additives, are subsequently eliminated upon thermal annealing. It is the case of methylammonium[28,29] or other monoammonium cations introduced in small quantities in 3D perovskites.[10] Therefore, we can suppose that the final average *n* is impacted by monoammonium or diammonium elimination upon thermal annealing. Because this point is at the origin of many biased conclusions in the literature, it is important to get a precise knowledge of the composition of the final annealed 2D HP films.

Herein, an easy-to-process and precise approach is presented for quantifying the cation composition within annealed perovskite layers. By dissolving them in deuterated DMSO-d_6 and analyzing the resulting solution using liquid ^{1}H NMR spectroscopy, we got precise quantifications of cationic species. Leveraging the integration of ^{1}H NMR spectrum peaks, the layer dissolution method (LDM) offers a straightforward and reliable manner to quantify individual cations with high precision. Our investigation reveals distinct behavior regarding the fate of RP monoammonium and DJ diammonium cations upon layers of thermal annealing. After thermal annealing, diammonium cations approach their initial quantities within the DJ perovskite layer, with a weak *n* increase. It results in a minimal change in the average *n* value after annealing for DJ perovskites, and low-dimensional phase content is high in the layers. In contrast, we have observed a notable reduction in the amount of monoammonium cations after annealing, leading to an increase in the average *n* value for the RP perovskite. This phenomenon is assigned to the deprotonation of the monoammonium cation and its subsequent volatilization. It results in a lower content in low-dimensional 2D RP perovskites phases and a higher quantity of high-dimensional phases. Consequently, their optoelectronic properties approach those of the 3D perovskites, while maintaining good stability thanks to the presence of a small amount of organic spacer cations. Furthermore, we show that the deprotonation-sublimation phenomenon is favored by the MACl additive which shifts the chemical equilibria.

2. Results and Discussion

2.1. 2D Perovskite Cations Quantification by Liquid 1H NMR Analysis

2.1.1. The Perovskite Precursor Solutions

^{1}H-NMR is a powerful technique to identify and quantify organic compounds. In preliminary experiments, to validate the accuracy of the technique, we first analyzed complex perovskite precursor solutions (PPSs) in DMSO-d_6. Liquid samples of perovskite precursors were prepared at room temperature, mixing A′I or A″I_2, PbI_2, FAI, and PbI_2. Their stoichiometry corresponded to 2D Dion-Jacobson A″$FA_5Pb_6I_{19}$ ($n = 6$) and 2D Ruddlesden-Popper

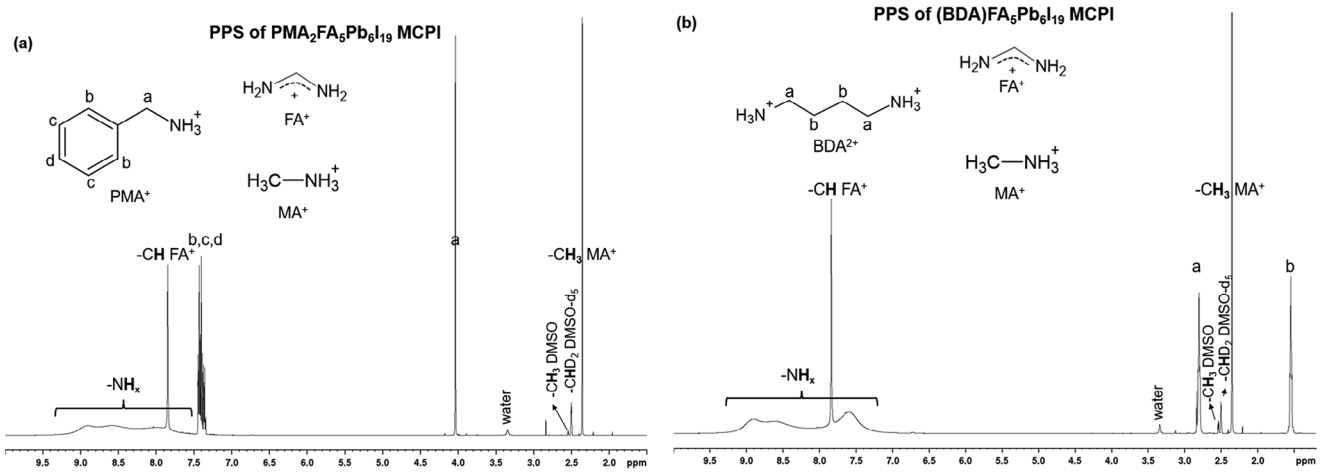

Figure 2. Examples of ^{1}H NMR spectra of precursor solutions: MACl.

$A'_2FA_5Pb_6I_{19}$ (n = 6). Moreover, due to the beneficial effects on final device performances (Tables S1–S4, Supporting Information), PbI_2 was added in excess, and MACl salt was also added (composition noted MCPI).[11] To draw conclusions as general as possible, we investigated four different A′ RP spacer cations: n-propylammonium (PA^+), n-butylammonium (BA^+), phenylmethylammonium (PMA^+) and 4-fluorophenethylammonium ($4FPEA^+$) and three different A″ DJ spacer cations: butane-1.4-diammonium (BDA^{2+}), 4-(aminomethyl)piperidinium ($4AMP^{2+}$) and 3-(aminomethyl)piperidinium ($3AMP^{2+}$). The molecular structures of A, A′ and A″ cations are shown in **Figure 1** with the proton indexation. The cations involved were quantified by integrating the peak intensity from characteristic signals in ^{1}H NMR spectra. The selection of these integrated signals was managed by recording ^{1}H NMR reference spectra (Figure S1, Supporting Information) and ensuring the absence of any overlapping signals that could affect their integrations.

The obtained spectra are shown in **Figures 2** and S2 (Supporting Information). Chemical shifts of the integrated signal of the A cations implemented in the inorganic frameworks (FA^+, MA^+), of A′ Ruddlesden-Popper organic spacer cations (PA^+, BA^+, PMA^+, and $4FPEA^+$) and A″ Dion-Jacobson organic spacer cations (BDA^{2+}, $4AMP^{2+}$, $3AMP^{2+}$) are provided in **Table 1**. The cation contents introduced in the PPSs by weighting and measured by ^{1}H NMR spectra are compared in Table S5 (Supporting Information). Notably, molar balance differences are anticipated to be more pronounced when measuring PPSs directly due to the large number of NH_x signals in the 7.0–9.0 ppm region, overlapping the formamidinium (FA^+) cation signal. For the latter, the average difference in molar balance between weighing and NMR measurement is 3.7%, which is rather elevated due to the selected signal location at 7.84 ppm within the NH_x signal region. Regarding spacer cations, the maximum difference was found for the propylammonium (PA^+) cations, with a molar difference of 4.9%, while the average difference across all spacer cations was 2.1%. Finally, for methylammonium MA^+, the average difference in molar balance was 2.2%. Overall, these values confirm the reliability of using ^{1}H NMR analysis for quantifying the cations present in the 2D HPs.

2.1.2. 2D Perovskite Layers Study

The next step was to prepare 2D RP and 2D DJ perovskite layers from precursor solutions with the various spacers. The methodology employed to prepare the NMR solution samples is schematized in **Figure 3**. Initially, the PPSs were spin-coated onto FTO-coated glass substrates covered by a thin compact titanium dioxide layer. The layers were then annealed for 15 min on a hotplate set at 153 °C and cooled down to room temperature. A total of 10 perovskite layers were dissolved in deuterated DMSO-d_6 and the resulting solutions were finally analyzed by ^{1}H NMR. The complete dissolution of perovskite layers in DMSO-d_6 was checked by measuring the sample absorption spectra before and after dissolution. Additionally, we confirmed that all cations were well-dissolved (Supplementary Note 1). The solutions of dissolved perovskite layers were highly stable and identical ^{1}H NMR spectra could be measured after several months (Table S6, Supporting Information). Details

Table 1. Identification of reference signals in ^{1}H NMR for different cations and their chemical shift.

Cation nature	Proton corresponding to the integrated signal	Chemical shift [ppm]
A-cation		
Formamidinium (FA^+)	Ha	7.84
A-cation/ Additive		
Methylammonium (MA^+)	Ha	2.37
Dion-Jacobson organic spacer cations		
Butane-1.4-diammonium (BDA^{2+})	Hb	1.59-1.51
4-(aminomethyl)piperidinium ($4AMP^{2+}$)	Hc + Hb	1.89-1.78
3-(aminomethyl)piperidinium ($3AMP^{2+}$)	He′	1.61-1.50
Ruddlesden-Popper organic spacer cations		
Phenylmethylammonium (PMA^+)	Ha	4.04
n-propylammonium (PA^+)	Hc	0.90
n-butylammonium (BA^+)	Hd	0.89
4-fluorophenethylammonium ($4FPEA^+$)	Hb	2.84

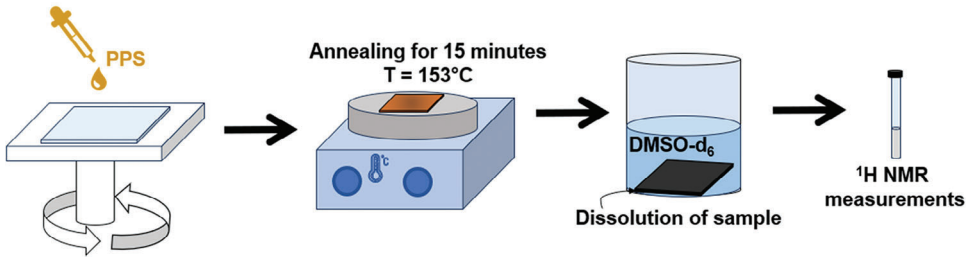

Figure 3. Schematic of the layer dissolution method (LDM) used for the NMR quantification of cations in perovskite layers.

regarding the methodology for cation quantification using ^{1}H NMR can be found in Supplementary Note 2. Error assessment was performed for each measurement, as detailed in Supplementary Note 3.

This layer dissolution method (LDM) offers distinct advantages over the traditional one of scratching perovskite films. First, the scratching method requires thicker perovskite layers. It can impact the thermal annealing of the perovskite layers and their final properties. Using LDM enables the preparation of perovskite layers with similar thicknesses and properties as the ones used for solar cells. Second, LDM ensures an accurate quantification without the risk of impurities contamination of the samples (no impurity NMR signal found). Finally, it proved to be more time-efficient compared to scratching.

For ^{1}H NMR spectra of annealed 2D Ruddlesden-Popper and 2D Dion-Jacobson perovskite layers dissolved in DMSO-d_6, two types of layers were analyzed: pristine (stoichiometric solutions without additives), and MCPI. Among the ^{1}H NMR spectra of pristine and MCPI layers, new peaks were detected, which were absent in the ^{1}H NMR spectra of PPSs directly prepared in DMSO-d_6. They have been assigned to reaction products between formamidinium and methylammonium, diammonium derivatives, or monoammonium derivatives as described in Supplementary Note 4. However, as these compounds were detected in very small amounts, generally, they have not been considered in the following of the paper.

2.2. 2D DJ and 2 RP Perovskite Layers

2.2.1. Study of Pristine 2D DJ and 2D RP Perovskite Layers

The cation molar balances of annealed layers of formamidinium (FA)-based 2D Dion-Jacobson (for BDA^{2+}, $4AMP^{2+}$ and $3AMP^{2+}$ spacers) and (FA)-based 2D Ruddlesden-Popper perovskites (for PA^+, BA^+, PMA^+ and $4FPEA^+$ spacers), prepared from stoichiometric solutions and denoted as pristine have been compared. Stoichiometric $A''FA_5Pb_6I_{19}$ (DJ) and $A'_2FA_5Pb_6I_{19}$ (RP) (n = 6) PPS compositions were utilized. **Figure** 4a shows that, for all 2D DJ perovskites, the quantity of organic spacer cations was slightly decreased after annealing, with a decrease larger than the error bars on NMR measurements. The initial ratio between the organic spacer and FA^+ for $n = 6$ is 20%. In the final annealed film, it reduced to 18% for BDA-based perovskites, 17% for 4AMP-based perovskites, and 19% for 3AMP-based perovskites. The final average n value (noted n_{DJ}) was calculated from NMR quantification:

$$n_{DJ} = \frac{x_{FA}}{x_{spacer}} + 1 \quad (1)$$

With x_{FA} the fraction of FA organic cation and x_{spacer} the fraction of spacer organic cation. It was slightly increased at ≈6.5 (Figure 4b). The reduction in the molar ratio of organic spacers with annealing was low, while the quantity of formamidinium remained unchanged, so the resultant effect on the n_{DJ} value was limited.

The same experiment was conducted with 2D Ruddlesden-Popper perovskite films. The initial ratio between the organic spacer and FA^+ for n = 6 is 40%. We found that the quantity of organic spacer cations clearly diminished upon annealing (Figure 4c). The PA-based perovskite exhibited the highest organic spacer content reduction, with a decrease from 39–40% before annealing to 25% after annealing. It was followed by PMA^+ (28%), $4FPEA^+$ (29%), and BA^+ (31%). The final average n (noted n_{RP}) was determined using the formula for 2D Ruddlesden-Popper:

$$n_{RP} = \frac{2x_{FA}}{x_{spacer}} + 1 \quad (2)$$

The reduction in x_{spacer} increased the final n_{RP} of pristine 2D Ruddlesden-Popper perovskite layers. Starting from a n of 6 in the PPS, PA-based perovskite layers yielded a final n_{RP} of 8.9. It was 8.1 for PMA-based perovskite, 7.8 for 4FPEA-based perovskite layers, and 7.4 for BA-based perovskite layers (Figure 4d). As no change in n was encountered when 2D RP perovskite layers were dissolved in DMSO-d_6 directly after spin-coating (Figure S11 and Table S8, Supporting Information), we can conclude that the increase in n is due to the spacer cation elimination, upon thermal annealing.

The elimination process of organic spacer cations in 2D RP perovskite layers upon thermal annealing involves a two-step mechanism, as illustrated in Figure 4e. Initially, the organic spacer cation A'^+ is deprotonated by interacting with I^- via an acid-base reaction. It results in the formation of the amine, noted A'^0, and of HI. Subsequently, A'^0 undergoes volatilization, concomitantly with the release of HI gas. Therefore, the elimination process relies on two important properties of the organic spacer cation: 1) the acid dissociation constant of A'^+/A'° couple (K_a),

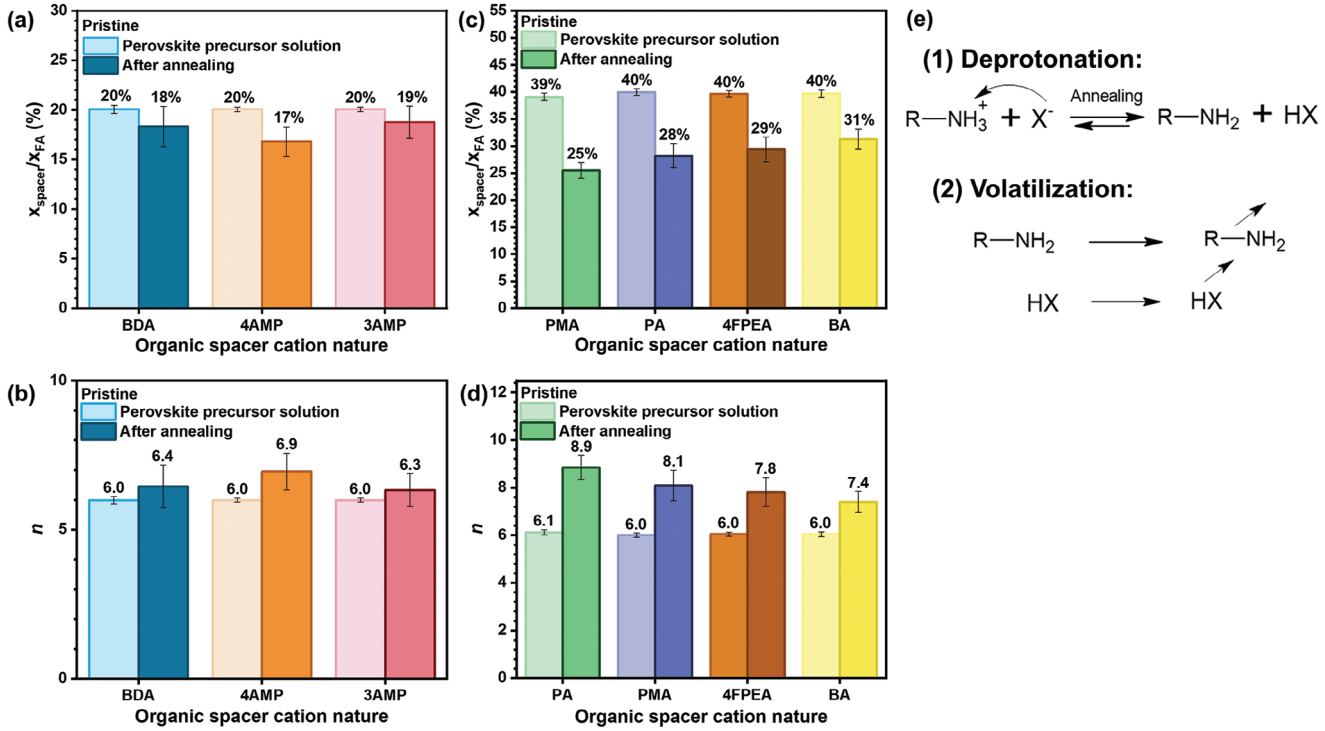

Figure 4. a) Ratio of organic spacer cation to FA^+ and b) *n* for precursor solution and film after annealing in pristine 2D Dion-Jacobson perovskite. c) Ratio of organic spacer cation to FA^+ cation and d) *n* for precursor solution and film after annealing in pristine 2D Ruddlesden-Popper perovskite. e) Reaction scheme of organic spacer cations deprotonation and volatilization process in 2D perovskite layer upon thermal annealing.

and 2) the volatility of its basic monoamine A′° form. Indeed, the propensity of a molecule to donate a proton is dictated by its pK_a, with lower pK_a values indicating a higher propensity to donate protons. The acid dissociation constant varies with temperature, as described by the van't Hoff equation:

$$\frac{d\ln(K_a)}{dT} = \frac{\Delta_r H^\circ}{RT^2} \tag{3}$$

Since acid dissociation is an endothermic reaction, the standard enthalpy of reaction ($\Delta_r H^\circ$) is positive. *R* is positive and represents the ideal gas constant and *T* denotes the absolute temperature. Consequently, as *T* rises, $\ln(K_a)$ increases, leading to a decrease in pK_A and an enhanced ability for the molecule to donate protons.[30] At the annealing temperature, A′$^+$ can be deprotonated. The initial pK_A depends on the molecule, creating differences in deprotonation ability between organic spacer cations. Tabulated values have been provided in H_2O at 25 °C and are reported in Table S9 (Supporting Information). They correspond to a different condition compared to the perovskite growing film ones but can be the basis for discussion. After deprotonation, the aptitude of the organic spacer cation to be eliminated from perovskite layers depends on the volatility of the formed monoamine or diamine compounds. Volatility depends on factors such as molecular weight, boiling point, intermolecular forces, and polarity. To compare RP organic spacer monoamine volatilities or DJ organic spacer diamine volatilities, boiling point is a good indicator and their values are given in Table S10 (Supporting Information).

The elimination of monoammonium in 2D RP perovskites surpasses that of diammonium in 2D DJ perovskites. It arises from the less energy bonding of the RP spacers compared to the DJ ones. 2D Ruddlesden-Popper perovskite structures rely on a van der Waals interaction between monoammonium cations and single hydrogen bonding between the inorganic frameworks and the monoammonium, rendering the crystal structure less stable compared to 2D Dion-Jacobson perovskites, where van der Waals interactions are absent, and diammonium cation is bonded to inorganic frameworks through two amino groups. Consequently, in the case of 2D Ruddlesden-Popper, the weaker interactions within the crystal lattice facilitate the monoammonium deprotonation and the volatilization of monoamine. Conversely, in the case of 2D Dion-Jacobson, the presence of two stronger hydrogen bondings makes the DJ spacer cation more stable. Deprotonation and volatilization of diamines are more challenging.

2.2.2. Role of Additives on 2D Dion-Jacobson Perovskite Layers Formation

Next, we conducted a comparative analysis of cation molar balances, determined by ^{1}H NMR, in annealed formamidinium (FA)-based 2D Dion-Jacobson layers prepared with 20 mol% excess of PbI_2 (based on PbI_2 content) and 48 mol% methylammonium chloride (MACl) (based on FAI content) additives (noted MCPI). These additives markedly enhance the power conversion efficiency (PCE) and stability of the solar cells. Notably, the addition of MACl is well-documented to help the crystallization of

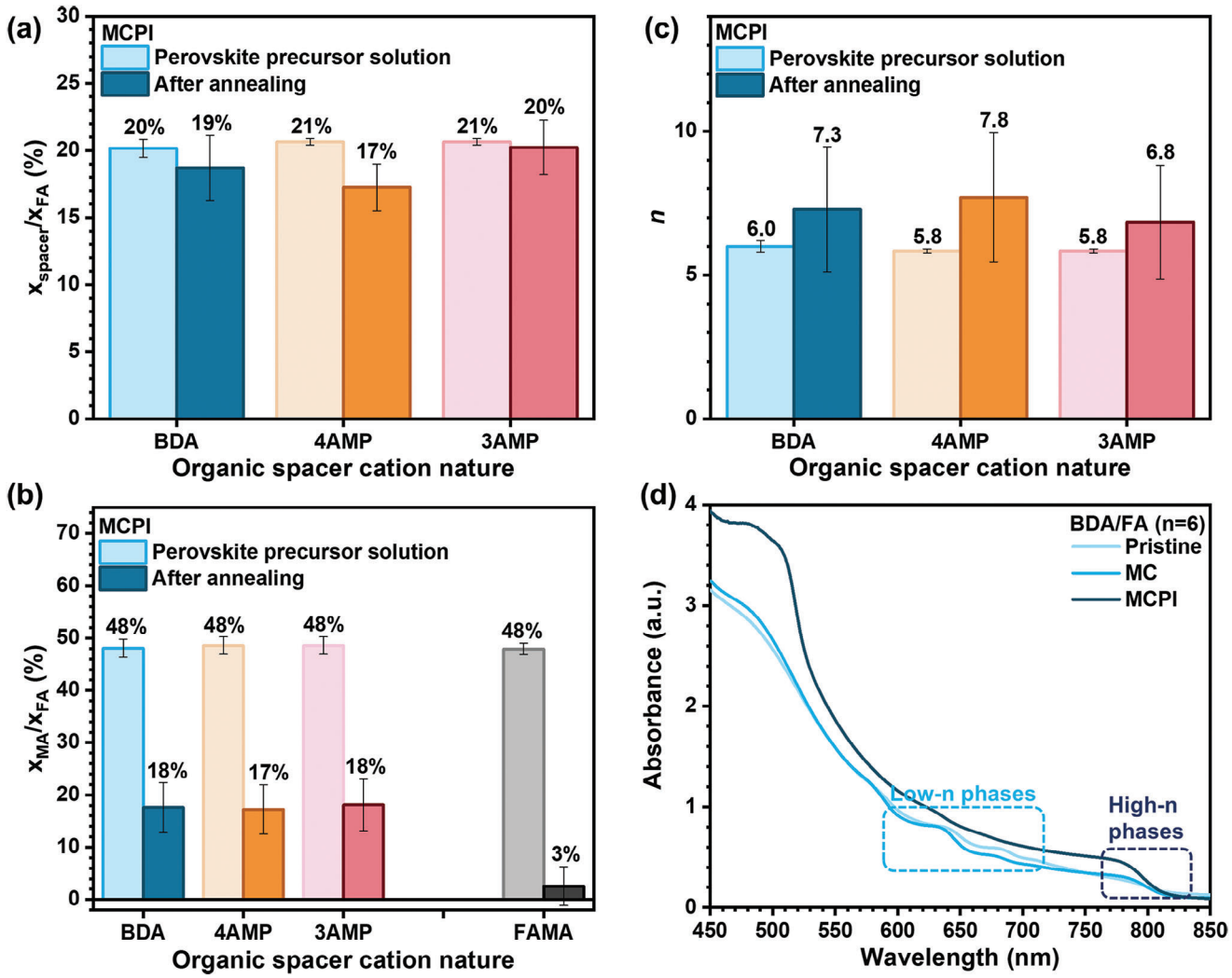

Figure 5. a) The ratio of organic spacer cation to FA^+ cation in MCPI 2D DJ perovskite for precursor solutions and for thermally annealed films. b) The ratio of MA^+ cation to FA^+ cation in MCPI 2D DJ perovskite for precursor solution and for thermally annealed films, and in 3D using FA^+ as cation in the A-site of the perovskite and only MACl as additive. c) Average *n* in MCPI 2D DJ perovskite for precursor solution and for films after thermal annealing. d) UV-vis absorbance spectra of pristine, MC, and MCPI BDA-based 2D DJ perovskite layers with initial $n = 6$.

the perovskite in its photoactive α-phase and PbI_2 fills defects and grain boundaries, thereby preventing non-radiative recombination (Tables S1 and S2, Supporting Information). To assess the specific contributions of each additive, layers were also fabricated using a PPS of $(BDA)FA_5Pb_6I_{19}$ with only methylammonium chloride additive (sample designated as MC).

Mirroring pristine layers, we observed a slight decrease in the ratio of organic spacer cations over FA^+ after annealing (**Figure** 5a). Starting from an initial 20% value, the final ratio was 19% for BDA-based perovskite layers. It was 17% and 20% for the 4AMP- and 3AMP-based perovskite layers, respectively. These very low reductions are assigned to the difficulty of deprotonating diammonium spacer cations during thermal annealing. While a small fraction of diamine spacers may volatilize, the majority of diammonium creates bonds with inorganic frameworks through two terminal hydrogen bonding and exhibits high boiling points. Consequently, there is no discernible change between pristine layers and MCPI layers, as methylammonium chloride and excess PbI_2 do not participate in this mechanism.

The evaluation of methylammonium MA^+ molar ratios was conducted by ^1H NMR analysis. Regardless of the organic spacer cation nature, the ratio of MA^+ to FA^+ markedly decreased upon annealing (Figure 5b). It was initially 48% in the PPS. It reduced, in the annealed layers, to 18% for BDA-based perovskites, 17% for 4AMP-based perovskites, and 18% for 3AMP-based perovskites. MA^+ cations underwent the same deprotonation process as spacer cations via an acid-base reaction with its chloride counterion. The pK_a value of the $MA^+/MA°$ couple at 25 °C in H_2O is 10.66. This value is close to the ones of PA^+/PA^0 (10.61) or BA^+/BA^0 (10.60) couples, while the HCl/Cl^- couple has a higher pK_a (−3.5) than the HI/I^- couple (−10) (Table S9, Supporting Information). This indicates that chloride is a stronger base with a greater deprotonation ability than iodide. Consequently, MA^+ linked with chloride during the precursor phase is more prone to deprotonation into methylamine (MA^0). Methylamine, with a

low boiling point of −6 °C (Table S10, Supporting Information) tends to volatilize immediately at annealing temperatures when no intermolecular interactions are involved. However, it has been observed that, in the case of MCPI 2D DJ perovskite layers, the decrease in molar ratio is not as pronounced as in 3D perovskite using FA^+ as the cation in the A-site and MACl as an additive (referred to as 3D-FAMA) (Figure 5b). In 3D-FAMA perovskites, the MA^+ to FA^+ ratio decreases from 48% before annealing to 3% after annealing (a small amount also served for the methylation of FA[27]) (Figure 5b). This discrepancy can be attributed to differences in intermolecular forces reducing the volatility of MA^+ in 2D DJ perovskites. To validate these findings, ^{1}H NMR analysis was conducted on MC BDA-based 2D DJ perovskites, revealing a decrease in MA^+ to FA^+ ratio from 48% before annealing to 5% after annealing (Figure S12a, Supporting Information). These results are further supported by tracking chloride content in annealed layers by the GD-OES technique. Chloride content can approximate MA^+ content in 2D DJ perovskite films because, during the precursor phase, no counterion exchange occurs between cations and the associated halide counterion attacks the proton of its cation, leading to subsequent volatilization of both compounds. This assessment is consistent with the Hard–Soft Acid–Base (HSAB) theory that hard bases interact with hard acids and soft bases interact with soft acids.[31] Notably, Cl^- is a harder base compared to I^-, and BDA^{2+}, with its dual positive charges and bulky organic chain, is softer than MA^+, with its smaller radius. Given this, BDA^{2+} associates with the softer base I^-, while MA^+ binds to the harder base Cl^-. Therefore, MA^+ content is equivalent to Cl^- content in the final layer, due to the absence of counterion exchanges. In MCPI annealed layers, chloride content is higher than in MC annealed layers, as depicted in Figure S12b,c (Supporting Information). Therefore, more methylammonium cations are eliminated when no excess PbI_2 is used.

GIWAXS measurements were conducted on both pristine and MCPI samples utilizing BDA^{2+} as an organic spacer cation (Figure S13a,c, Supporting Information), as well as on a BDA-based 2D DJ perovskite using only excess PbI_2 as an additive (PI sample) (Figure S13b, Supporting Information). In the pristine sample, a predominant ring of high-n and (111) 2D phase orientation is observed, accompanied by a ring corresponding to δ-phase. This yellow phase arises from the large FA^+ cation, prompting crystallization in the orthorhombic phase. The PI sample exhibited an additional ring, indicative of unreacted PbI_2 due to its excess in the PPS. Remarkably, in the MCPI sample, both the PbI_2 ring and δ-phase ring vanished, suggesting that smaller MA^+ cations react with an excess of PbI_2 to form inorganic frameworks in the 2D perovskite layer. Consequently, the MA^+ ratio should be considered when calculating the average n of the annealed layer, as MA^+ is incorporated within the inorganic framework of the perovskite.

Next, n_{DJ} was calculated for the MCPI 2D DJ annealed layers through the molar fractions of organic cations measured by ^{1}H NMR:

$$n_{DJ} = \frac{x_{FA} + x_{MA}}{x_{spacer}} + 1 \quad (4)$$

Figure 5c compares the initial n in the PPS, calculated from the weighting data, and the n_{DJ} in the annealed layers. Starting from 5.8-6, n increased to 7.3, 7.8, and 6.8 in BDA-based, 4AMP-based, and 3AMP-based final samples, respectively. This slight increase is attributed to methylammonium remaining in the layer which reacts with excess PbI_2 to form more organic/inorganic perovskite frameworks. For MC-only BDA-based perovskite, the final average n_{DJ} is calculated to be 6.8, rather close to the initial average n due to significant methylammonium elimination, as shown in Figure S12d (Supporting Information).

These findings are corroborated by the absorbance spectra of pristine, MC & MCPI BDA-based perovskite layers, as illustrated in Figure 5d. Specifically, pristine and MC layers, characterized by low final n_{DJ}, present pronounced absorbance peaks at shorter wavelengths demonstrating a high presence of low-n phases, whereas they present a low absorption edge at longer wavelengths indicating a low presence of high n-phases. Both pristine and MC layers exhibit a mixture of phases, which favors an inhomogeneous phase distribution within the layer. Conversely, for MCPI layers, with higher final n_{DJ}, a stronger absorbance edge at longer wavelengths is evident, with a weak absorbance peak at shorter wavelengths, suggesting that a higher content of high-n phases is present within the MCPI layers. The phase distribution in the MCPI layer is more homogeneous than in both pristine and MC layers, which is beneficial for charge transfer through the layer and leads to a lower ratio of non-radiative recombination.

2.2.3. Role of Additives on 2D Ruddlesden-Popper Perovskite Layers Formation

The next step was to investigate the cation molar balances in annealed layers of formamidinium (FA)-based 2D RP perovskites layers prepared in the presence of additives. These layers are referred to as MCPI. A stoichiometry of $A'_2FA_5Pb_6I_{19}$ (average initial n = 6) was utilized to prepare the PPSs. We employed 20 mol% excess of PbI_2 (compared to PbI_2 content) and 40 mol% methylammonium chloride (MACl) (compared to FAI content), as they demonstrated enhancement of performance and stability of PSCs. Notably, on the one hand, smaller cation MA^+ helps to crystallize the perovskite in its photoactive α-phase and PbI_2 fills the defects and grain boundaries, and, on the other hand, a combination of both additives helps to control solvent elimination and favorable growth orientation, as shown by Liu et al.[11] The optimal molar ratios of each additive were determined on PMA-based perovskite solar cells to achieve the best additive concentration, as shown in Tables S3 and S4 (Supporting Information).

The four PA^+, BA^+, PMA^+, and $4FPEA^+$ organic spacer cations A′ were investigated. The organic cations were quantified by LDM and ^{1}H NMR methods. In **Figure 6a**, the ratios of organic spacer cations to FA^+ exhibit significant decreases after annealing. Among the various types of organic spacer cations, the most pronounced reduction is found for PMA-based perovskite layers, with a decline from an initial 40% in PPS to 6% in the final layer. It is followed by PA-based perovskite layers at 14%, 4FPEA-based perovskite layers at 18%, and BA-based perovskite layers at 19%.

When compared to pristine 2D Ruddlesden-Popper perovskite layers (Figure 4c), the reduction in the organic spacer cation to FA^+ ratio is more pronounced in the presence of additives. This indicates that the addition of methylammonium chloride

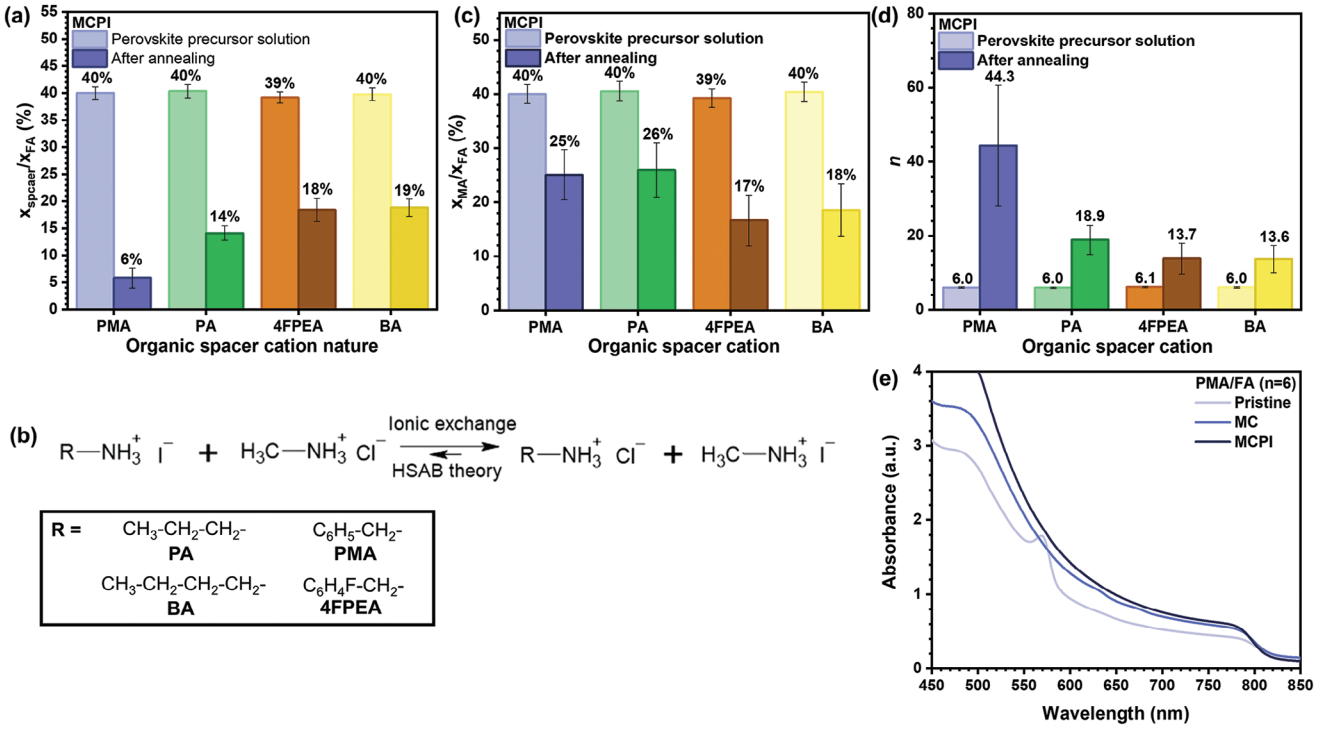

Figure 6. a) Ratio of organic spacer cation to FA^+ cation in MCPI 2D RP PPS and for films after annealing. b) Reaction scheme of counterion exchange during the layer preparation. c) The ratio of MA^+ cation to FA^+ cation in MCPI 2D RP PPS and for films after annealing. d) Average *n* of MCPI 2D RP PPS and for films after annealing. e) UV–visible absorbance spectra of pristine, MC, and MCPI PMA-based 2D Ruddlesden-Popper perovskite layers with an initial average *n* of 6.

and excess PbI_2 increases the organic spacer cation elimination. Conversely, to diammonium spacers, monoammonium spacer cations (MSCs) have a similar acid-basic hardness to methylammonium. Therefore, during the layer preparation, we can suppose that exchanges of counterions occur between methylammonium and MSCs, based on the HSAB theory.[31] The counterion exchange reaction between methylammonium and the MSC is illustrated in Figure 6b. At the end of the precursor phase, it is anticipated that approximately equal amounts of methylammonium iodide and methylammonium chloride are present, as well as equal contents of monoammonium iodide and monoammonium chloride. Monoammonium chloride is easier to deprotonate than monoammonium iodide (Table S9, Supporting Information), leading to more deprotonations occurring in the case of MCPI layers compared to pristine layers, thereby explaining the subsequent increase in volatilization for MCPI layers.

An interesting observation is that the elimination of organic MSCs depends on their nature. As discussed above, the elimination process of organic spacer cations depends on two key factors. First, the acid dissociation constant value (pK_a) of monoammonium / monoamine couples (Table S9, Supporting Information) governs the first step of deprotonation by counterion via acid-base reversible reaction. The PMA^+/PMA° couple has the lowest pK_a, facilitating extensive deprotonation and, thus, explaining the predominant elimination of PMA^+ cations. PA^+ cations are eliminated to a high extent, despite the relatively high pK_a associated with PA^+/PA° couple, indicating fewer deprotonations for PA^+ cations. This observation suggests that volatility must also be considered to understand the elimination of organic spacer cations. In Table S10 (Supporting Information), PA^0 exhibits the lowest boiling point, indicating that when PA^+ is deprotonated, it easily volatilizes. Moreover, PA^0 small size enables its easier diffusion through the perovskite layer than other investigated monoammonium cations. The elimination of $4FPEA^+$ cations and BA^+ cations are similar but occur preferentially for different reasons. $4FPEA^+$ cations are expected to undergo a higher rate of deprotonation than BA^+ due to a lower pK_A. However, $4FPEA^0$ possesses a high boiling point, resulting in reduced volatility and decreased organic spacer elimination. Since deprotonation is a reversible reaction, $4FPEA^0$ that is not volatilized can be protonated again into $4FPEA^+$. On the other hand, BA^0 has a lower boiling point, increasing its volatility. The combination of these two phenomena helps to explain the similar organic spacer to FA^+ ratios after thermal annealing.

The evaluation of methylammonium MA^+ molar ratios was conducted by ^1H NMR signals quantification. Across all organic spacer cation types, the ratio of MA^+ to FA^+ underwent a decrease after annealing, as depicted in Figure 6c. Starting from an initial 40% in the PPS, this ratio decreased to 25% in PMA final layer, 26% in PA-based perovskite layers, 17% in 4FPEA-based perovskite layers, and 18% in the BA-based perovskite layers. The MA^+ to FA^+ ratios of MCPI 2D RP perovskite layers experienced a smaller decrease after annealing compared to MCPI 2D DJ perovskite layers. It is explained by a chloride exchange with monoammonium occurring solely in the case of RP monoammonium cations. Consequently, a mixture of MACl and MAI is

present in the precursor phase. MACl is easier to deprotonate than MAI (Table S10, Supporting Information), leading to reduced deprotonation in 2D RP compared to 2D DJ, and, subsequently, to less volatilization. Similar to the behavior observed in 2D DJ perovskites, MA^+ cations in 2D RP perovskites strongly interact with excess PbI_2, thereby preventing their volatilization. Indeed, for MC PMA-based perovskite layers, stronger MA^+ elimination is evident, as shown in Figure S14a (Supporting Information), where MA^+ to FA^+ ratio decreases from an initial 40% to 13% in the final layer.

The chloride content in 2D RP MC and MCPI PMA-based perovskite layers was evaluated through the integration of their GD-OES profile (Figure S14b,c, Supporting Information). Despite MA^+ being only partially eliminated, the chloride content is significantly reduced. This observation confirms that most chloride content has been used to deprotonate cations, spacers, or methylammonium, and subsequently volatilized. Additionally, it supports the notion that chloride can indeed deprotonate RP monoammonium cations. The final n_{DP} of 2D RP perovskite layers was estimated based on cation molar fractions determined by ^{1}H NMR measurements, as:

$$n_{RP} = \frac{2(x_{FA} + x_{MA})}{x_{spacer}} + 1 \quad (5)$$

The results are reported in Figure 6d. The highest n_{RP} was reached for PMA-based perovskites going from 6.0 before annealing to the high 44.3 value after annealing. It is caused by the strong deprotonation due to the acid character of PMA^+ cations. For PA-based perovskites, the final n_{RP} was 18.9, partly because of PA^0 high volatility. It was 13.7 and 13.6 for the 4FPEA-based and the BA-based final perovskites, respectively.

These findings are supported by the absorbance spectra of pristine, MC & MCPI PMA-based perovskite layers, as illustrated in Figure 6e. The former, characterized by the lowest final average n_{RP} of 8.1 (Figure 4d), presents pronounced absorbance peaks at shorter wavelengths demonstrating a high presence of low-n phases, whereas it presents a low absorption edge at ≈800 nm, indicating a low presence of high n-phases. MC layers had a final n_{RP} of ≈38 due to the high elimination of organic spacer cations and partial elimination of MA^+ cations. Their absorbance at longer wavelengths is increased due to the appearance of more large-n phases in the final layer. Despite the higher presence of the high-n phase, some low-n phases remain, resulting in an inhomogeneous phase distribution. Finally, for MCPI layers with the highest final n_{RP} of 44, a strong absorbance edge at ≈800 nm is present, suggesting that only high-n phases are present within the MCPI layers. It results in a more homogenous phase distribution compared to pristine and MC layers, which is advantageous for charge transfer through the perovskite layer.

2.3. Organic Spacer Cations Elimination Tracking upon Annealing and Study of the Initial N

PMA-based RP perovskite layers with 36 mol% MACl (based on FAI content) were annealed at different times and analyzed by LDM and ^{1}H NMR to quantify the evolution of cations molar fractions. The decreases in PMA^+ and MA^+ molar fractions and the increase of FA^+ molar fraction over the annealing time are depicted in **Figure 7a**. PMA^+ and MA^+ exhibit similar behavior regarding their elimination kinetics. The PMA^+ elimination process is fast during the first two minutes of annealing and then slows down up to 10 min. At the beginning of annealing, numerous low-*n* phases are present as shown by the high PMA^+ molar fraction. Gradually, the decomposition of low-*n* phases occurs due to the deprotonation of PMA^+ into PMA^0, with Cl^- anion promptly attacking the acid. A minor part of deprotonated MA^+ reacts with FA^+ to form MFA^+, as described in our previous work.[28] The change in MFA^+ content with annealing time is reported in Figure S10b (Supporting Information). This compound is formed in a small amount during the first annealing minute and, then, does not evolve.

The impact of the initial *n* value was also investigated. MC PMA-based 2D RP perovskites with different *n* values (*n* = 2/3/5/9/100), all with 36 mol% of MACl additive (based on FAI content), were analyzed using LDM and liquid ^{1}H NMR analysis. From the analysis results in Figure 7b, it is evident that the relative decrease in (x_{MA}+x_{PMA}) to x_{FA} in the final layer increases with the initial *n*. This suggests that the less PMA^+ is introduced, the more it is eliminated. This has consequences on MA^+ because MACl is introduced at the same concentration regardless of the initial quantity of PMA^+. Therefore, more Cl^- anions interact with PMA^+ in lower *n* perovskites, leaving fewer Cl^- ions to deprotonate MA^+, leading to fewer deprotonations and volatilization (Figure 7c). Indeed, PMA^+ is more deprotonated than MA^+ due to the lower pK_a value of PMA^+/PMA° couple, compared to MA^+/MA° couple (Table S9, Supporting Information).

The final average *n* was calculated, as shown in Figure 7d. For *n* = 1, the final *n* remains 1 because only PMA^+ is introduced, so even though it is eliminated through deprotonation with I^-, it still leads to a *n* = 1 phase. For *n* = 2 and *n* = 3, the final average *n* increases to 3 and 5 respectively, resulting in quasi-2D perovskites. For *n* = 5 and *n* = 9, the final average *n* increases to 13 and 84, respectively. In the case of n = 100, the PMA —CH_2 signal was below the ^{1}H NMR limit of detection because its final quantity was too low. This implies that PMA^+ is almost fully eliminated upon thermal annealing in that case.

We finally investigated the consequence of partial spacer elimination on the solar cell performances. Devices employing a direct configuration of glass/FTO/compact TiO_2/mesoporous TiO_2/perovskite/Spiro-OMeTAD/Au, as illustrated in **Figure 8a**, were fabricated. Based on the previous study, we prepared 2D RP and 2D DJ perovskites in the presence of additives showcasing a final *n* of 13 after thermal annealing. This enabled us to investigate whether the main parameter determining the final power conversion efficiency of a 2D PSC is the final average *n*.

The *J–V* curves in Figure 8b offer a representative insight into the performances of the solar cells, with corresponding photovoltaic parameters summarized in **Table 2**. For PMA-based solar cells, a V_{oc} of 1.075 V, J_{sc} of 20.49 mA cm^{-2}, *FF* of 61.64%, and PCE of 13.58% were achieved. In contrast, the BDA-based solar cell exhibited a V_{oc} of 0.922 V, J_{sc} of 16.86 mA cm^{-2}, *FF* of 67.26%, and a PCE of 10.46%. Despite equivalent final average *n*, it is evident that 2D DJ-based PSCs display lower V_{oc} and J_{sc}, compared to 2D RP-based PSCs, resulting in a lower PCE. This decrease is attributed to the lower crystallinity observed in BDA-based 2D DJ perovskite layers, as evidenced by the reduced

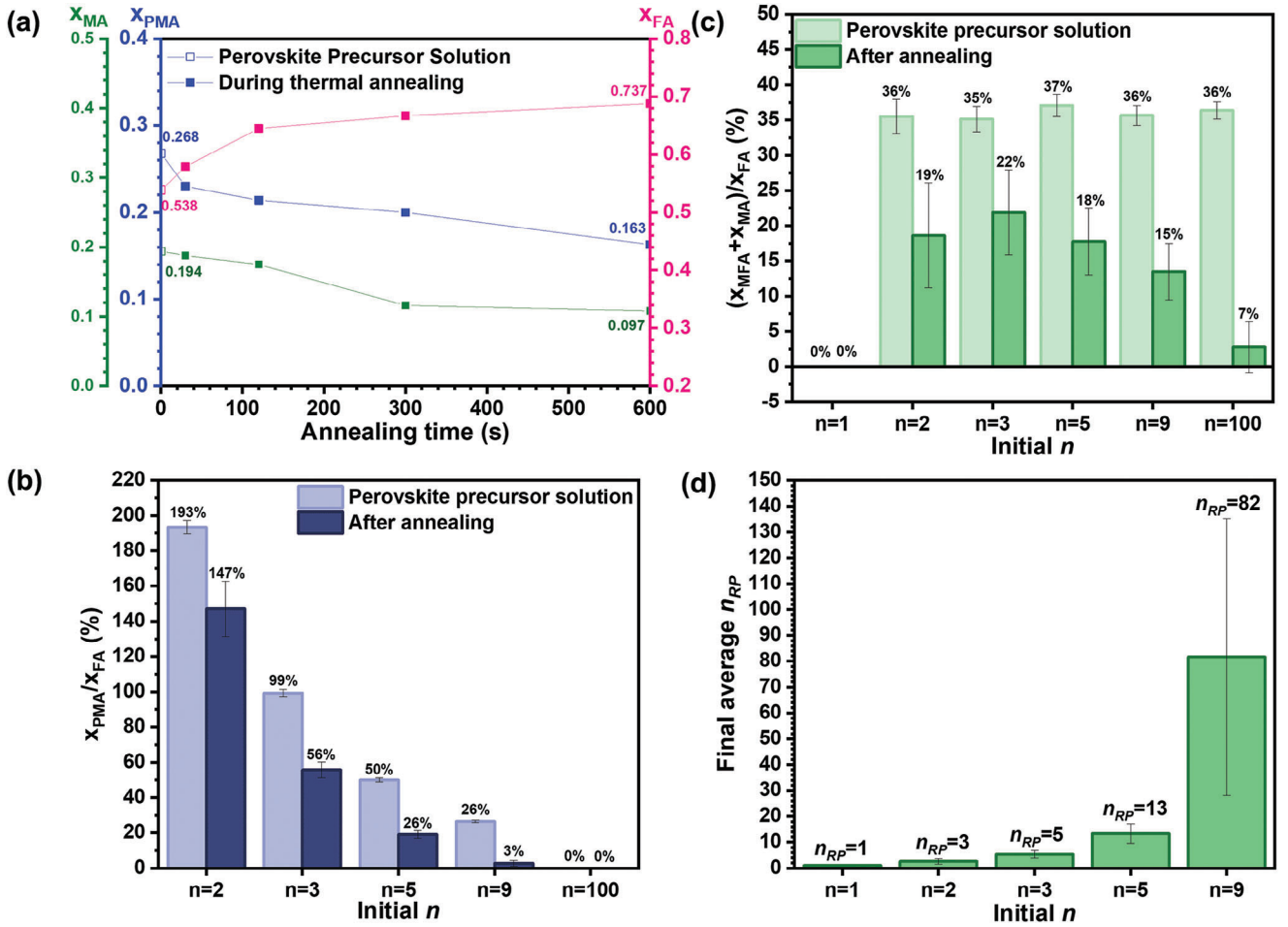

Figure 7. a) Evolution of PMA^+, FA^+, and MA^+ molar ratios upon thermal annealing for MC PMA-based 2D RP perovskite layers. b) PMA^+ to FA^+ ratio in PPS and in final MC PMA-based 2D RP perovskite layers for different initial n values. c) (MA^+ + MFA^+) to FA^+ ratio in PPS and in final MC PMA-based 2D RP perovskite layers for various initial n values in the PPS. d) Final average n_{RP} of MC PMA-based 2D RP perovskite layers prepared from different initial n values in the PPS.

peak intensity in XRD patterns (Figure S15a, Supporting Information). Notably, while the diffractogram of the BDA-based perovskite layer shares similar peak positions with 3D FAMA perovskite (Figure S15b, Supporting Information), it exhibits lower peak intensity. XRD diffractogram of PMA-based perovskite layer exhibits three peaks at 6.57°, 9.83°, and 13.14° corresponding to the (040), (060), and (080) crystal planes of $n = 3$, and one peak at 8.6° corresponding to the (040) crystal plane of $n = 2$. Another strong peak near 13.96° corresponds to the (111) crystal plane of the high-n phase. It indicates that the PMA-based perovskite

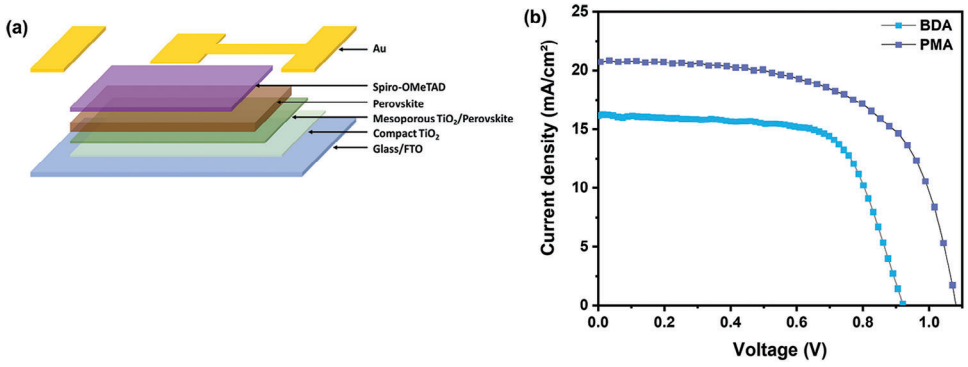

Figure 8. a) Schematic view of the PSC structure. b) *J–V* curves of PMA-based and BDA-based solar cells, prepared with MACl additive to get the same final $n = 13$.

Table 2. Photovoltaic parameters of PMA-based and BDA-based solar cells with the same final $n = 13$.

Sample	Scan direction	V_{oc}/V	J_{sc}/mA/cm^2	FF/%	PCE/%	HI/%
2D RP PMA-perovskite with $n = 13$	Reverse	1.075	20.49	61.64	13.58	16.6
	Forward	1.069	20.52	51.57	11.31	
2D DJ BDA-perovskite with $n = 13$	Reverse	0.922	16.86	67.26	10.46	14.4
	Forward	0.854	16.68	62.83	8.95	

layer displays a mixture of low-n phases and high-n phases that can be detrimental to the performance of solar cells. These results are consistent with absorbance spectra that display an absorbance band edge at ≈800 nm due to large-n phases and absorption peaks at shorter wavelengths due to low-n phases (Figure S15c,d, Supporting Information). More surprisingly, BDA-based 2D DJ perovskite with a final average n of 13 demonstrated a more significant absorption at ≈800 nm than PMA-based 2D RP perovskite or 3D FAMA perovskites. It also displays a small absorption peak at shorter wavelengths confirming the presence of low-n phases, which could impede carrier transportation. The enhanced light absorption of BDA-based perovskite layers may positively impact the J_{sc} of solar cells. Consequently, the lower J_{sc} and V_{oc} values observed in DJ-based perovskite indicate the presence of defects induced by diammonium cations, which adversely affect charge carrier generation and transportation, primarily through recombination processes. Thus, the detrimental effect of diammonium cations in perovskite layer quality is underscored by these J-V curve parameters.

3. Conclusion

We have developed the quantification via liquid ^{1}H NMR of organic cations present in 2D Ruddlesden-Popper and in 2D Dion-Jacobson perovskites thin films. This method is shown easy to implement, efficient, and precise. Upon the layer thermal annealing, diammonium in 2D DJ perovskites is little eliminated due to reduced deprotonation and lower volatility of the resulting molecules that have a high boiling point and are bounded by rather strong intermolecular forces. They can further interact with the crystal lattice. Conversely, monoammonium in 2D RP perovskites is eliminated via a two-step deprotonation and volatilization process. The phenomenon is favored by a lower pK_a value and a higher volatility of spacer cations. The addition of methylammonium chloride in the precursor solution leads to halide ions exchange with the spacer. Cl^- has a higher aptitude to deprotonate than I^-. It results in a higher elimination of the spacer while MA^+ is partially incorporated into the crystal lattice. The formed compounds have a higher n value compared to the pristine case. This phenomenon is much more pronounced in 2D RP than in 2D DJ perovskites. We have then shown that the solar cell PCE difference between the two perovskite types cannot be solely attributed to variations in the final average n. Instead, differences in crystallinity, defect formations, and morphology create differences in carrier transportation and non-radiative recombination rates, explaining PCE variations. Our work provides an important insight into the chemistry of the 2D perovskite layers preparation. It unveils neglected aspects of their formation mechanism and final properties, and it shows the importance of determining their "true" average n value.

Supporting Information

Supporting Information is available from the Wiley Online Library or from the author.

Acknowledgements

The ANR agency is acknowledged for financial support via the ChemSta project ANR-21-CE05-0022. Prof. Peter Siffalovic's group (Slovak Academy of Science, Bratislava, Slovakia) is acknowledged for GIWAXS measurements. Ile de France Region is acknowledged for financial support of the 500 MHz NMR spectrometer of Chimie-ParisTech in the framework of the SESAME equipment project (no. 16016326).

Conflict of Interest

The authors declare no conflict of interest.

Data Availability Statement

The data that support the findings of this study are available in the supplementary material of this article.

Keywords

2D halide perovskite film formation, nuclear magnetic resonance, solar cells, spacer cation volatilization, thermal annealing

Received: July 29, 2024
Published online: August 29, 2024

[1] H. Gu, J. Xia, C. Liang, Y. Chen, W. Huang, G. Xing, *Nat. Rev. Mater.* **2023**, *8*, 533.
[2] M. Liu, T. Pauporté, *Nano-Micro Lett.* **2023**, *15*, 134.
[3] F. Zhang, K. Zhu, *Adv. Energy Mater.* **2020**, *10*, 1902579.
[4] W. Chi, S. K. Banerjee, *Trends Chem* **2022**, *4*, 1005.
[5] S. Liu, Y. Guan, Y. Sheng, Y. Hu, Y. Rong, A. Mei, H. Han, *Adv. Energy Mater.* **2020**, *10*, 1902492.
[6] T. T. Ava, A. Al Mamun, S. Marsillac, G. Namkoog, *Appl. Sci.* **2019**, *9*, 188.
[7] Y. Fan, H. Meng, L. Wang, S. Pang, *Sol. RRL* **2019**, *3*, 1900215.
[8] J.-W. Lee, Z. Dai, T.-H. Han, C. Choi, S.-Y. Chang, S.-J. Lee, N. De Marco, H. Zhao, P. Sun, Y. Huang, Y. Yang, *Nat. Commun.* **2018**, *9*, 3021.

[9] T. Yang, L. Gao, J. Lu, C. Ma, Y. Du, P. Wang, Z. Ding, S. Wang, P. Xu, D. Liu, H. Li, X. Chang, J. Fang, W. Tian, Y. Yang, S. Liu, K. Zhao, *Nat. Commun.* **2023**, *14*, 839.
[10] J. Liang, Z. Zhang, Y. Huang, Q. Xue, Y. Zheng, X. Wu, C. Tian, Y. Zhang, Y. Wang, Z. Chen, C.-C. Chen, *Adv. Funct. Mater.* **2022**, *32*, 2207177.
[11] M. Liu, D. Zheng, T. Zhu, K. Vegso, P. Siffalovic, T. Pauporté, *Adv. Mater. Interfaces* **2024**, *11*, 2300773.
[12] L. Mao, W. Ke, L. Pedesseau, Y. Wu, C. Katan, J. Even, M. R. Wasielewski, C. C. Stoumpos, M. G. Kanatzidis, *J. Am. Chem. Soc.* **2018**, *140*, 3775.
[13] M. Shao, T. Bie, L. Yang, Y. Gao, X. Jin, F. He, N. Zheng, Y. Yu, X. Zhang, *Adv. Mater.* **2022**, *34*, 2107211.
[14] G. Wu, T. Liu, M. Hu, Z. Zhang, S. Li, L. Xiao, J. Guo, Y. Wang, A. Zhu, W. Li, H. Zhou, Y. Zhang, R. Chen, G. Xing, *Adv. Mater.* **2023**, *35*, 2303061.
[15] X. Li, J. M. Hoffman, M. G. Kanatzidis, *Chem. Rev.* **2021**, *121*, 2230.
[16] S. Ahmad, X. Guo, *Chin. Chem. Lett.* **2018**, *29*, 657.
[17] J. Gong, M. Hao, Y. Zhang, M. Liu, Y. Zhou, *Angew. Chem., Int. Ed.* **2022**, *61*, e202112022.
[18] Y. Chen, Y. Sun, J. Peng, J. Tang, K. Zheng, Z. Liang, *2D Ruddlesden-Popper perovskites for Optoelectronics* **2018**, *30*, 1703487.
[19] C. Liang, D. Zhao, Y. Li, X. Li, S. Peng, G. Shao, G. Xing, *Energy Environ. Mater.* **2018**, *1*, 221.
[20] J. Liu, J. Leng, K. Wu, J. Zhang, S. Jin, *J. Am. Chem. Soc.* **2017**, *139*, 1432.
[21] G. Xing, B. Wu, X. Wu, M. Li, B. Du, Q. Wei, J. Guo, E. K. L. Yeow, T. C. Sum, W. Huang, *Nat. Commun.* **2017**, *8*, 14558.
[22] P. Cheng, Z. Xu, J. Li, Y. Liu, Y. Fan, L. Yu, D.-M. Smilgies, C. Müller, M. Zhao, S. F. Liu, *ACS Energy Lett.* **2018**, *3*, 1975.
[23] J. Yang, C. Li, X. Wei, Y. Huang, D. Wu, J. Lai, M. Pi, L. Luo, X. Tang, *Appl. Phys. Lett.* **2024**, *124*, 011106.
[24] C. M. Soe, W. Nie, C. C. Stoumpos, H. Tsai, J.-C. Blancon, F. Liu, J. Even, T. J. Marks, A. D. Mohite, M. G. Kanatzidis, *Adv. Energy. Mater.* **2017**, *8*, 1700979.
[25] W. Ke, L. Mao, C. C. Stoumpos, J. Hoffman, I. Spanopoulos, A. D. Mohite, M. G. Kanatzidis, *Adv. Energy Mater.* **2019**, *9*, 1803384.
[26] S. Ahmad, M. Guan, J. Kim, X. He, Z. Ren, H. Zhang, H. Su, W. C. H. Choy, *Adv. Energy Mater.* **2023**, *14*, 2302774.
[27] X. Zhao, T. Liu, A. B. Kaplan, C. Yao, Y.-L. Loo, *Nano Lett.* **2020**, *20*, 8880.
[28] D. Zheng, F. Chen, M.-N. Rager, L. Gollino, B. Zhang, T. Pauporté, *Adv. Mater. Interfaces.* **2022**, *9*, 2201436.
[29] T. Zhu, D. Zheng, M.-N. Rager, T. Pauporté, *Sol. RRL* **2020**, *4*, 2000348.
[30] M. Wang, Z. Shi, C. Fei, Z. J. D. Deng, G. Yang, S. P. Dunfield, D. P. Fenning, J. Huang, *Nat. Energy* **2023**, *8*, 1229.
[31] Q. A. Akkerman, V. D'Innocenzo, S. Accornero, A. Scarpellini, A. Petrozza, M. Prato, L. Manna, *J. Am. Chem. Soc.* **2015**, *137*, 10276.